Chapter 10

Design and Characterization of EUV and X-ray Multilayers

Hui Jiang

Additional information is available at the end of the chapter

http://dx.doi.org/10.5772/62385

Abstract

Multilayers, which consist of periodic/aperiodic nanometer-scale stacks of two or more alternating materials, fill a gap between visible light optics and natural crystal by realizing high near-normal incidence reflectivity in extreme ultraviolet and soft X-ray regions and diffraction-limited focusing in hard X-ray region. Before fabricating a multilayer, it is essential to design a structure that realizes the required optical features. The optimization process uses merit functions that are defined by the design targets. In this chapter, the designs of two typical aperiodic multilayer structure, X-ray supermirror and EUV beam splitter, are introduced. Precision characterization of multilayer structures is the key process in multilayer sciences as well in order to improve fabricating process and determine optical properties in use. Searching a most suitable structure model to approaching real one by comparing experimental and simulated results is essentially an optimization problem. In this chapter, by fitting the X-ray grazing incidence reflectivity and diffuse scattering curves, the realistic multilayer structures are determined accurately.

Keywords: multilayer, merit function, downhill simplex, particle swarm optimization, reflectivity

1. Introduction

As we all know, mirror and lens are capable of realizing high reflectivity and focusing in visible light regime (wavelength λ=~400–760 nm). But the situation is very different in X-ray and extreme ultraviolet (EUV) regimes. In soft X-ray (λ=~1–10 nm) and EUV (λ=~10–100 nm) regimes, the absorption for all materials is strong enough so that conventional type of mirror is unable to realize high reflectivity near normal incidence, meanwhile the natural crystal does not work as

well due to small lattice constant. In hard X-ray regime, because the refractive indices for most materials are close to unify, it is impossible to use lens to focus X-rays.

Multilayers, consisting of periodic/aperiodic nanometer-scale stacks of two or more alternating materials deposited on a substructure, fill the gap between mirror and crystal by realizing high near-normal incidence reflectivity in EUV [1, 2] and soft X-ray [3, 4] regimes, and also challenge diffraction-limited focusing in hard X-ray regime by multilayer Kirkpatrick-Baez [5] or multilayer Laue lens [6] systems.

The history of multilayers is from the 1940s. Initial attempts to fabricate Ag/Cu periodic structures failed due to their serious interdiffusions [7]. Twenty years later, stable Fe/Mg periodic structures were first made [8]. In 1972, Spiller [3] found that a mirror consisting of two alternate materials with different refractive indices can increase the near-normal incidence reflectivity in the EUV and soft X-rays regimes. In the 1980s, Vinogradov [9] and Barbee [10] developed relative theories of multilayers and, in 1992 Yamamoto [11] developed an intuitive and effective design method. Since the 1980s, as a result, the ultra-precise manufacture and technologies of thin films were rapidly improved to promote the development of multilayers. Typical bilayer periodic pairs for different energy regions are Mo/Si [2], W/B_4C [12], Cr/C [13], Mo/Y [14], and Mg/SiC [15], etc. Aperiodic multilayers, developed more recently, can provide tailored spectral requirements, such as broadband or broad-angle high reflectivities [16, 17], high integral throughput [18], broadband polarizers [19, 20] and chirped mirrors [21, 22]. Such multilayers have wider applicability than periodic multilayers and natural crystals.

Nowadays, multilayers have presented wide applications in many important fields. In semiconductor industry, multilayers were used in mask illumination and replication [1] for next-generation extreme ultraviolet lithography. In synchrotron field, multilayers were always considered as key components for reflection [4], polarization [23], focusing [24] and monochromatization [25]. Biology imaging was often used at water window regime (λ=2.3–4.4 nm) based on excellent contrast by using multilayer near-normal reflection [26] or required higher energy resolution to avoid spot blurs [27]. In addition, multilayers were also recorded in significant applications like space telescope [28], plasma diagnosis [29], neutron science [30], etc.

In this chapter, design and characterization of EUV and X-ray multilayers are presented. Optimization algorithms play important roles in these works. They help us to find optimal structures to satisfy any required spectral performances and based on experimental curves to retrieve real structure information.

2. Multilayer model

The optical behavior in a periodic multilayer can be described by a corrected Bragg equation with constant periodic thickness D, fractional thicknesses of absorber (scattering) layers d_a and spacer layers d_s and complex refractive indices $n_a=1-\delta_a+i\beta_a$ and $n_s=1-\delta_s+i\beta_s$,

http://dx.doi.org/10.5772/62385

$$m\lambda = 2D\sin\theta\left[1-\frac{2(d_a\delta_a + d_s\delta_s)}{\sin^2\theta}\right]^{1/2} \tag{1}$$

where m is the reflection order, λ is the wavelength and θ is the gracing incidence angle. For a multilayer with two materials of similar absorption, the highest reflectivity (in the first reflection order) requires the thickness of each layer to be close to a quarter of the wavelength.

For a periodic/aperiodic multilayer with a substrate of finite thickness, the reflectance and transmittance coefficients at each interface can be calculated using the Fresnel equations which, for the j^{th} interface, can be written as

$$\begin{aligned}
r'_{p,j} &= \frac{n_{j-1}\cos\theta_j - n_j\cos\theta_{j-1}}{n_{j-1}\cos\theta_j + n_j\cos\theta_{j-1}} \\
r'_{s,j} &= \frac{n_{j-1}\cos\theta_{j-1} - n_j\cos\theta_j}{n_{j-1}\cos\theta_{j-1} + n_j\cos\theta_j} \\
t'_{p,j} &= \frac{2n_{j-1}\cos\theta_{j-1}}{n_{j-1}\cos\theta_j + n_j\cos\theta_{j-1}} \\
t'_{s,j} &= \frac{2n_{j-1}\cos\theta_{j-1}}{n_{j-1}\cos\theta_{j-1} + n_j\cos\theta_j}
\end{aligned} \tag{2}$$

where n_j is the refractive index of the j^{th} layer, θ_j is the incidence angle in that layer and s and p refer to the two polarizations. The s- and p-component amplitude reflections and transmissions also can be expressed using the recurrence formula [31]

$$\begin{aligned}
r_j &= \frac{r'_{j+1}E_{j+1} + r_{j+1}\exp(-2i\delta_{j+1})}{1 + r'_{j+1}E_{j+1}r_{j+1}\exp(-2i\delta_{j+1})} \\
t_j &= \frac{t'_j t_{j-1}\exp(-i\delta_j)}{1 + r'_j E_j r_j\exp(-2i\delta_j)}
\end{aligned} \tag{3}$$

where δ_j is the phase factor of the j^{th} layer and E_j is the roughness factor of the j^{th} interface, normally the Debye-Waller factor $\exp(q_j^2\sigma_j^2/2)$ or the Nevot-Croce factor $\exp(q_j q_{j+1}\sigma_j^2/2)$ [32], where q is the wave vector and σ is the root mean square (RMS) interfacial roughness. For smooth interfaces, the Nevot-Croce factor was considered to be better than the Debye-Waller factor. In applying equation 4, the thickness of the substrate is usually considered to be infinite, and so the initial conditions are r_{n+2}=0 and t_0=1 as shown in **Figure 1**. The recurrence formula can then be used to calculate r_0 and t_{n+2}. The reflectance R and transmittance T in an n-layer multilayer system can be expressed as

$$R_{\mathrm{p/s}} = \frac{R_{0,\mathrm{p/s}}}{T_{0,\mathrm{p/s}}} = r_{\mathrm{p/s},0} r^{*}_{\mathrm{p/s},0}$$
$$T_{\mathrm{p/s}} = \frac{T_{n+2,\mathrm{p/s}}}{T_{0,\mathrm{p/s}}} = t_{\mathrm{p/s},n+2} t^{*}_{\mathrm{p/s}.n+2} \tag{4}$$

The scattering signal is around the specular direction. The scattering potential is divided into a non-disturbed part and a disturbance. Interferences of reflected and transmitted waves have four types of interaction based on the dynamic scattering process [33]. The whole diffuse scattering signal is represented as

$$I_{diff} = I_0 \Delta\Omega / 2 \cdot A_s / A_b \sum_{j,k=1}^{N} \left| n_j^2 - n_{j+1}^2 \right|^2 \cdot \sum_{m,n=0}^{3} S_{j,k}^{mn}(q_x) \tilde{G}_j^m (\tilde{G}_k^n) \exp\left\{ -\frac{1}{2} \left[\left(q_{z,j}^m \sigma_j \right)^2 + \left(\left(q_{z,k}^n \right)^* \sigma_k \right)^2 \right] \right\} \tag{5}$$

where $\Delta\Omega$ is the detector acceptance angle, A_s/A_b is the area ratio of the radiation on the sample to beam spot, $G^m{}_j$ is the four mutual products of T_i(or R_i) and T_s(or R_s) and $S(q_x)$ is the structure factor.

$$S_{j,k} = \int_0^{\infty} C_{j,k}(x) \cos(q_x x) \mathrm{d}x \cdot \exp\left(-\left| Z_j - Z_k \right| / \xi_{\perp} \right) \tag{6}$$

where $\xi_{\perp}$ is the vertical correlation length and $C(x)$ is the lateral correlation function which is based on the self-affine characteristic of rough interface [34] and $\xi_{//}$ is the lateral correlation length and h is the fractal exponent.

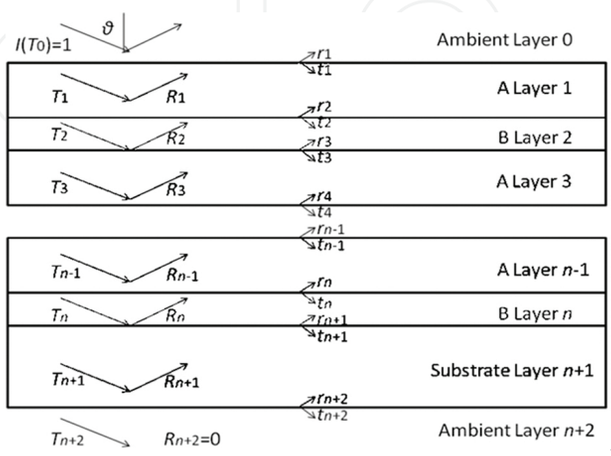

Figure 1. Reflectance and transmittance coefficients at each interface of a multilayer structure.

http://dx.doi.org/10.5772/62385

3. Optimization algorithm

3.1. Introduction

Normally, before using a multilayer, it included three important steps: design, fabrication and characterization. It is essential to design a structure that realizes the required optical features before the multilayer fabrication. Fabrication technologies, such as sputtering and evaporation, are typical random processes. Their technology parameters need to be attempted and optimized repeatedly. The attempts are based on accurate structural characterization. The most effective structural characterization methods are hard X-ray grazing incidence specular reflectance (XRR) and diffuse scattering (XDS). The experimental curve can be compared to the simulated curve calculated from a guessed multilayer model until reach a satisfying agreement. It is clear whether design or characterization, the core is optimization algorithm. Suitable optimization algorithms enable us to search optimal multilayer structure in design and determine the most realistic multilayer structure in measurement.

In general, optimization algorithms include local and global optimizations. The former refers to situations in which an approximate range of optimal values is known prior to the optimization. If a group of candidate structures can be defined at the outset, it is straightforward to find optimal structures in a short time. Common local algorithms are mainly based on the least gradient, including quasi-Newton method [35], steepest-descent method [36], Levenberg–Marquardt algorithm [37, 38], downhill simplex algorithm [39], etc. In the design of aperiodic multilayers, several techniques have been developed to search for initial candidate structures, including Kozhevnikov's method [17] and the search for suitable positions and numbers of layers such as needle optimization [40, 41], in order to make these local algorithms converge to better results.

The global algorithm has a larger search space and so always takes more time to search for the optimal structure than a local algorithm does, but prevents local results that miss the global optimum. Global algorithms play a more significant role than local algorithms because of their wider search ranges and stronger search capabilities. Global algorithms, often based on natural phenomena and processes, include random search (RS) [42], genetic algorithms [43] (GA), simulated annealing (SA) [44], differential evolution [45], hybrid multistate (MS), topographical optimization [46], particle swarm optimization (PSO) [47] and the ant colony optimization (ACO) algorithm [48].

Many optimization algorithms have been used in multilayer design. According to different requirements, different optimization targets are chosen as the functions to estimate the pros and cons of the algorithm. This kind of function is defined as merit functions. The balance between calculation time and search accuracy needs to be considered when choosing a suitable optimization algorithm.

3.2. Downhill simplex algorithm

The downhill simplex algorithm (Nelder-Mead method) [49] is a typical local optimization. The method only requires function evaluation and not derivatives. It is based on a movable

simplex with N+1 vertices in N dimensions (N variables). In two dimensions, the simplex is a triangle.

The optimization is started with the N+1 vertices defining an initial simplex. If one of these vertices is defined as the starting point $\mathbf{P}_0$, the other N vertices can be expressed as $\mathbf{P}_i=\mathbf{P}_0+\tau\mathbf{e}_i$, where e_i is a unit vector and τ is a constant defining the characteristic length scale. The coordinates of the vertices define the current multilayer structure, and the merit function of each vertex can be calculated. Most optimization steps move the vertex of the simplex with the best merit function through the opposite face of the simplex to a lower vertex. These basic steps are called reflections. The center of the reflection is the weighted center of the simplex based on the merit function of each vertex. If the merit function of the reflected vertex is better than that of the best vertex in the previous step, this reflection direction can be regarded as the correct one and the reflection can be doubled, which is called expansion. In contrast, if the reflected vertex is worse than the previous worst vertex, the simplex should move along the transverse reflection direction – this is called inward contraction. If the reflected vertex is just better than the worst previous vertex, the reflection rate should be halved, which is called contraction. Based on these steps, the simplex moves toward a valley in the solution. When the merit functions of all the vertices are sufficiently close, the optimal multilayer structure can be considered to have been found.

3.3. Particle swarm optimization

The PSO algorithm, one of the most important swarm intelligence methods, is a parallel evolutionary computation technique developed by Kennedy and Eberhart in 1995 [47]. The motivation of PSO was to understand the behavior of birds or fish searching for food. The process is similar to GA, but only has a few operators, including selection, crossover and mutation. Any particle moves with its own velocity, which is updated according to its own experience and that of the other particles. Some studies [50] have shown that in PSO the inertia weight (defined following equation 8) influences the trade-off velocities between global and local exploration abilities, and in GA crossover and mutation have different effects at the beginning and end of the process. The one-way information transfer means that PSO convergences to best solution faster than GA, in which the whole swarm moves uniformly. PSO also has stronger ergodicity than GA and is the only evolutionary algorithm that does not incorporate survival of the fittest.

In an N-dimension objective space (N variables for optimization), there are M particles to search for the optimal solutions. The location and velocity of the i^{th} particle are defined by groups of candidate solutions

$$\begin{cases} X_i = (X_{i1}, X_{i2}, \cdots, X_{iN}) \\ V_i = (V_{i1}, V_{i2}, \cdots, V_{iN}). \end{cases} \tag{7}$$

For the design of multilayers, the location variables are the layer thicknesses and the working angle. For the characterization, the variables can be the layer thicknesses, densities, roughness,

http://dx.doi.org/10.5772/62385

material interdiffusions, etc. The velocity expresses the search direction of any particle, which updates the new location and velocity at the next iteration to be

$$\begin{cases} V_i(k+1) = wV_i(k) + c_1r_1(p_i(k) - X_i(k)) + c_2r_2(g(k) - X_i(k)) \\ X_i(k+1) = X_i(k) + V_i(k+1). \end{cases} \quad (8)$$

The new velocity includes inertia, cognitive and social learning terms. The inertia term forces a particle to tend to follow its old velocity, including an inertia weight w which influences the trade-off between global and local exploration abilities, changing from w_{max} = 0.9 at the beginning to w_{min} at the maximum iteration. In the cognitive and social learning terms, c_1 and c_2 are acceleration constants and r_1 and r_2 are random numbers uniformly distributed in the interval (0,1). The functions $p_i(k)$ and $g(k)$ are, respectively, the previous best location for the i^{th} particle and the previous best locations for all particles at the k^{th} iteration. These two terms guarantee that every particle can extract its own experience and share information from the society, making faster converge at the beginning of a run. "The behavior of any particle can be sketched in **Figure 2**."

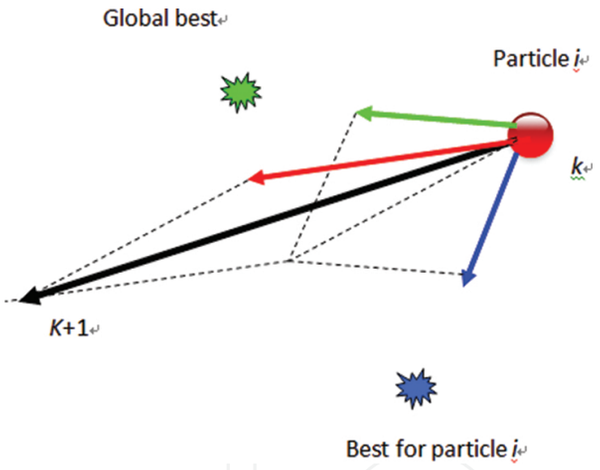

Figure 2. The searching process of one particle.

The basic process of the algorithm is as follows: Step 1 is the random initialization of locations and velocities. The ranges of possible locations are selected using a priori knowledge. The maximum velocities should be about 20% of the location range in any step. If the velocities are too large, the particles in the next iteration can fly beyond the location boundary. If they are too small, the convergence rate is very low. The merit function of each particle is then determined and the optimum one is sought. Step 2 is the update of locations and velocities to the next iteration according to equation 8. If any location is beyond the boundary, it is replaced by the boundary value and the velocity direction is reversed, analogous to reflection from a wall. The merit functions of the particles are then calculated and the best location of each particle and the best global location are updated. Step 3 is the inspection of the defined convergence

condition. If this is satisfied or the set maximum number of iterations have taken place, the program terminates. Otherwise step 2 is repeated.

If the other parameters are fixed, a smaller $w_{\min}$ can increase the speed of convergence, but the optimization is more likely to fall into a local optimum solution. Following an analysis of the relationship between parameter selection and convergence [51], large $w_{\min}$ close to $w_{\max}$ and relatively small acceleration constants of about 0.3–0.7 were chosen to make the whole optimization converge effectively. For a larger number of variables (e.g., more than two materials), more particles and more iterations have to be used.

4. Design of multilayers

4.1. Introduction

The usual design targets are reflectivity, transmitivity and phase performance. Simple periodic multilayer structures are suitable for single wavelengths or working angles, but more complicated aperiodic structures are needed to tailor spectral or phase responses. In general, the optimization process uses merit functions that are defined by the design targets. The selection of suitable multilayer materials, based on optical constants and material stability, is the starting point of the design process. The optimization of particular designs is complicated and can only be enabled using various computer algorithms. An important technological constraint is that the optimal structure should be as simple as possible, avoiding ultra-thin layers and drastically variable layer thicknesses.

In this section, the designs of two typical aperiodic multilayers, respectively, X-ray supermirror and EUV intensity beam splitter, based on my PhD studies [52], are presented to show the important role of optimization algorithm on multilayer design.

4.2. X-ray supermirror

Supermirrors are aperiodic multilayers often used in X-ray [53] or neutron [54] imaging systems. They are designed to provide particular characteristics such as increased reflectivity or flat optical response over broader angular or energy ranges than possible with conventional periodic multilayer mirrors. Based on these characteristics, they have been chosen for use in X-ray telescope [55] and applications of synchrotron radiation [56].

In this study, a broad-angle supermirror will provide relatively high peak reflectivity over a wide angular range and several times the integrated reflectivity.

The principle of supermirror design is also based on the Bragg diffraction equation. Compared to a periodic multilayer mirror with fixed layer thicknesses and thickness ratios, a broad-angle supermirror with variable periodic thickness and thickness ratio provides the interference effect of the standing waves over a range of working angles. The target of the design is to obtain high average reflectivity and small reflectivity fluctuations over a defined angular range. The merit function for such designs is

http://dx.doi.org/10.5772/62385

$$F = \min \sum_{i=1}^{j} (R_j - R_{\text{target}})^2 \tag{9}$$

where j is the number of working angles at which the reflectivity is calculated and R_{target} is the target for the average reflectivity.

There are two methods to define the initial multilayer structures in the optimization. The first is to determine the periodic structure related to the center of the working angular range. The second is based on Kozhevnikov's study [17], which is an analytic method that gives an approximate initial depth-graded structure to enable a faster approach to the optimum solution. This method has been applied to various broad-angle [57] and broadband [58] designs of multilayer mirrors. The expression for the reflectivity of a depth-graded multilayer mirror is

$$\begin{aligned} R(\lambda) &= |r(\lambda)|^2 = \left| \frac{2\eta(\lambda)\sqrt{|q'(z)|}}{\eta^2(\lambda) + |q'(z)|} \right| \exp\left(-4\kappa_2(\lambda) z\right) \\ \eta(\lambda) &= \frac{(\varepsilon_1(\lambda) - \varepsilon_2(\lambda))\sin(\pi\Gamma)}{2\lambda\sqrt{\mu(\lambda) - \cos^2\theta}}. \end{aligned} \tag{10}$$

where $q(z)$ (which describes the multilayer structure) is positive, continuous and differentiable, L is the total multilayer thickness, and ε_1 and ε_2 are the dielectric permittivities of the two materials. μ is the mean dielectric permittivity, $\kappa = k(\mu - \cos^2\theta)^{1/2}$ where k is the wave vector. κ_2 is the imaginary part of κ. Alternatively, for a given target reflectivity, the multilayer structure $q(z)$ can be determined by solving the inverse problem.

A Cr/B_4C supermirror was designed for chromium K_α radiation and incidence angles in a range around 2°, the latter to fit within the structure of the X-ray microprobe source. **Figure 3(a)** shows the design results for an angular width of 0.14°. Using downhill simplex algorithm, the design was close to the initial depth-graded structure and easily fabricated. Mostly, the thickness ratios of the layer pairs are between 0.32 and 0.34. **Figure 3(b)** shows the change from the initial reflectivity to the optimal value. **Figure 4(a)** and **(b)** show the influences of using different initial structures. Although the reflectivity curves are similar, the optimal structures from the initial periodic structures have larger fluctuations that lead to more difficulties in fabrication, since rapidly varying thicknesses make it hard to ensuring correct deposition rates. **Figure 5** and **Table 1** show designs for different angular ranges. Supermirrors can increase the angular width by several times and, although the maximum reflectivity decreases substantially, the overall reflectivity for all angles used in the optimization increases.

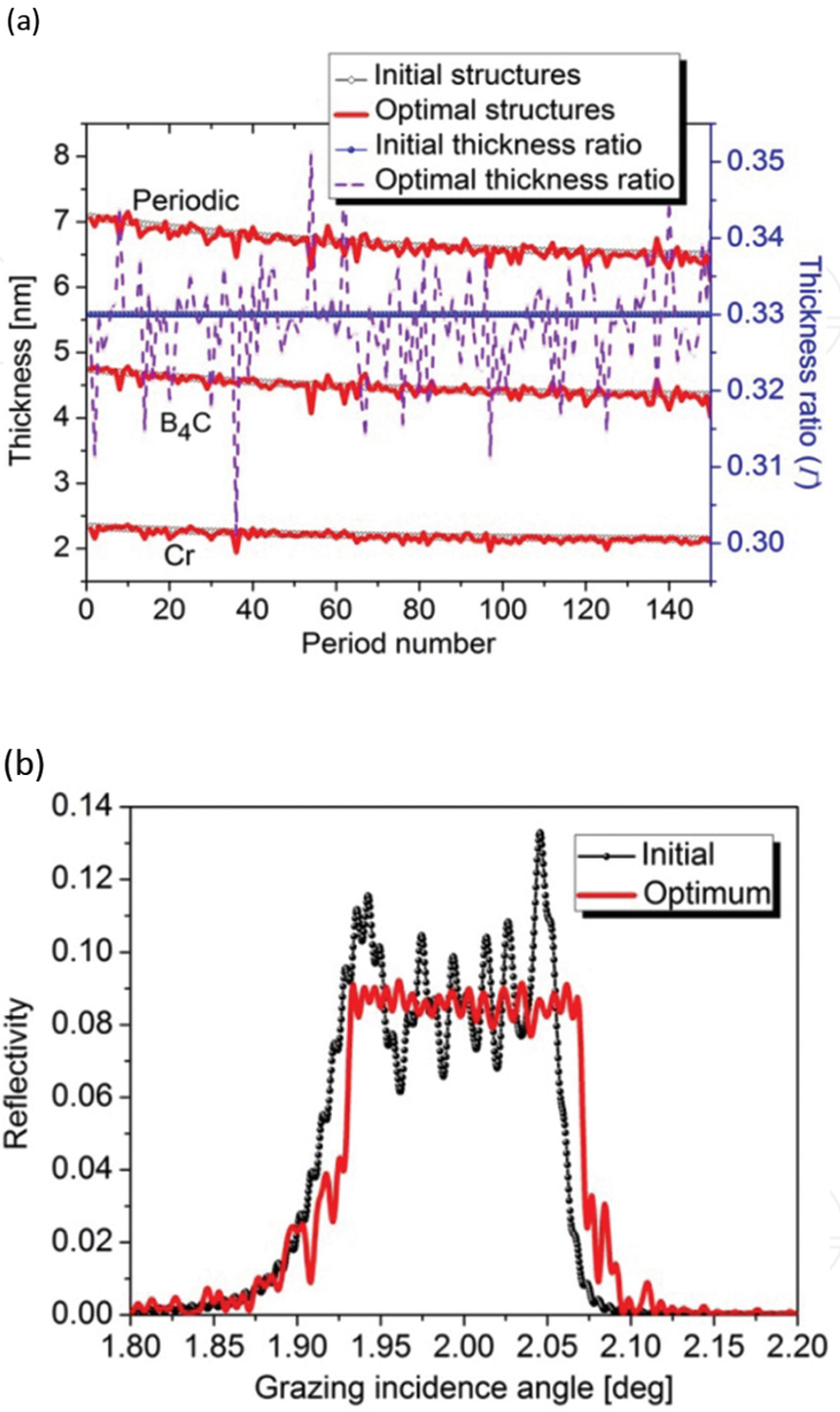

Figure 3. (a) The initial and optimized layer thicknesses for a Cr/B_4C aperiodic multilayer mirror with an angular width of 0.14°. (b) Comparison of the reflectivity curves for the initial and optimum structures.

http://dx.doi.org/10.5772/62385

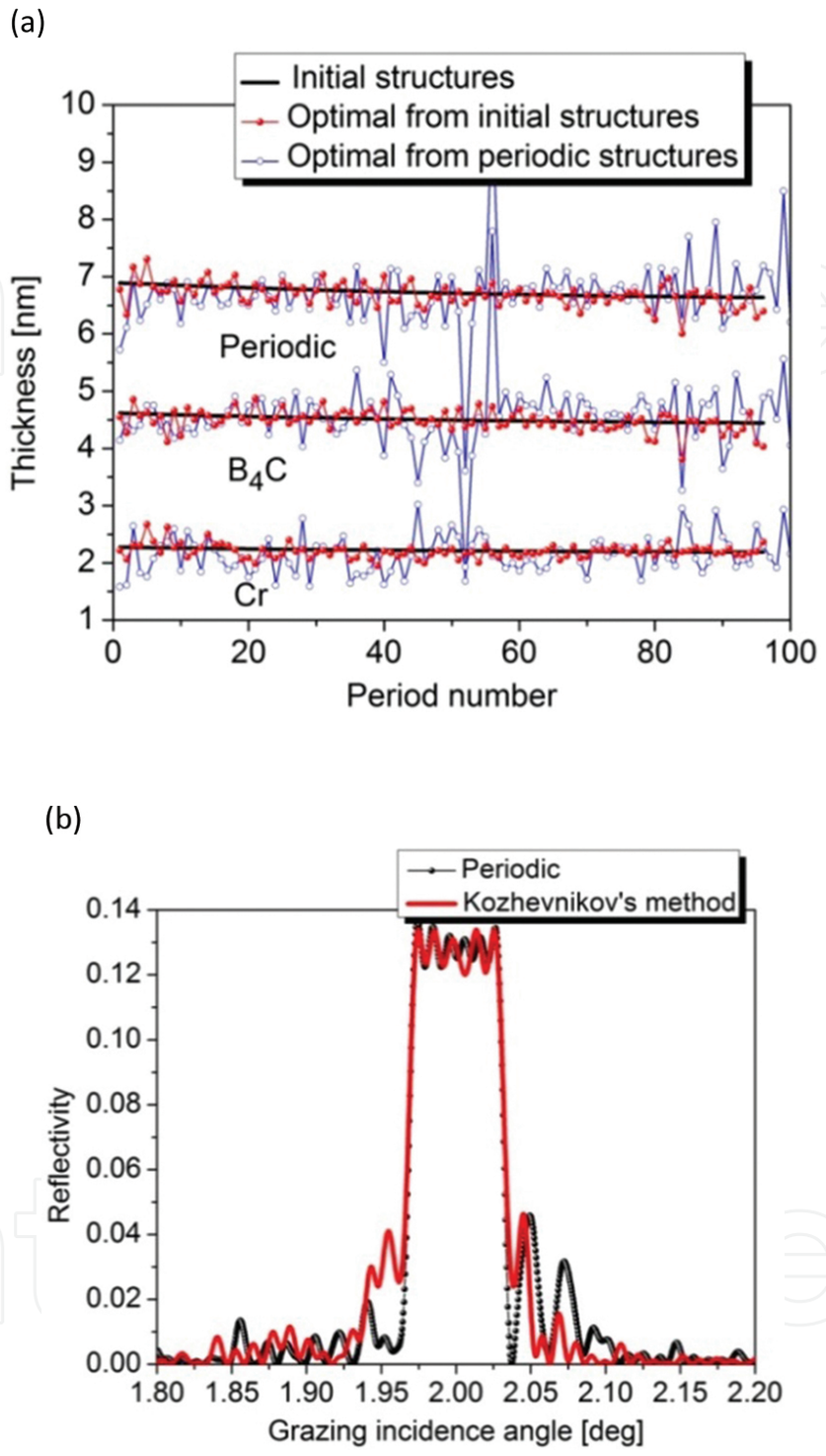

Figure 4. (a) The thicknesses of Cr/B_4C aperiodic multilayer mirrors for different initial structures. (b) Comparison of the optimum reflectivity curves for the two initial structures.

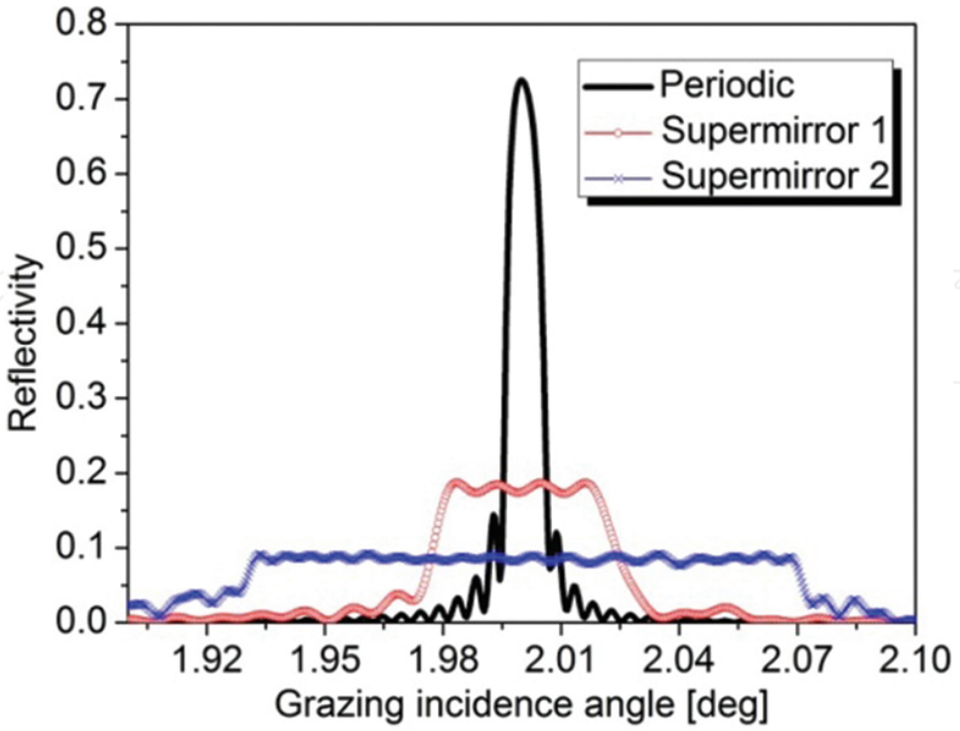

Figure 5. Different angular width requirements lead to different optimum results reflectivity profiles.

Sample	FWHM [deg]	Peak Reflectivity [%]	Overall Reflectivity
Periodic	0.01	71.4	0.008
Supermirror 1	0.05	18.0	0.010
Supermirror 2	0.15	8.4	0.014

Table 1. Comparison of FWHM, peak reflectivity and integrated reflectivity for two aperiodic supermirrors and a periodic multilayer.

4.3. EUV intensity beam splitter

A large amount of work has been done on multilayers for mask illumination and replication [1, 59] in extreme ultraviolet lithography (EUVL), but so less thought has been given to inspection of the masks and produced components. Defects in EUVL masks can occur in both the absorber patterns and the multilayer-coated mask blanks, and inspection is essential as the number of defects has to be minimized. However, conventional full-field or scanning imaging is not appropriate as the masks and components are too absorbing to the radiation. An alternative is to use interferometry [60] like Schwarzschild optics [61]. A multilayer beam splitter divides an incident beam into two coherent parts by reflecting part and transmitting part, respectively, reflected from a sample multilayer and a reference multilayer. Interference fringes are produced when they are recombined.

http://dx.doi.org/10.5772/62385

There is a trend to utilize broadband spectrum from the source based on tine or xenon plasmas instead of single wavelength around 13nm to irradiate wafers, in order to decrease exposure times [62]. Hence, broadband beam splitters optimized to the output of tin or xenon plasmas are required.

The merit function must satisfy two requirements for an intensity beam splitter: (1) high reflectance and transmittance throughputs and (2) excellent agreement between the reflected and the transmitted beam intensities over the range of wavelengths. The merit function chosen was

$$F = \sum_{i=1}^{m} \frac{\left[R(\lambda_i) - T(\lambda_i)\right]^2}{R(\lambda_i) + T(\lambda_i)} \tag{11}$$

where m is the number of wavelength calculation points. The squared numerator ensures good agreement between the intensities and the denominator prevents the intensities from becoming too small.

The principle of material choice for beam splitters is a little different from that for high-reflectivity multilayers. The differences in the optical constants are more important for high reflectivity, while the absorption coefficients have more influence for beam splitters. Since silicon nitride is used as the substrate, due to its high strength, stability and transmittance, the transmitted beam is affected by the silicon absorption edge at 12.4 nm. Ruthenium and molybdenum are suitable for the scattering layers and beryllium, yttrium and silicon can be chosen for the spacer layers. Among their pairs, Mo/Si [63] and Mo/Be [64] have been widely studied for use at 13.5 and 11.4 nm. In this design, Mo/Si was chosen as the material pair.

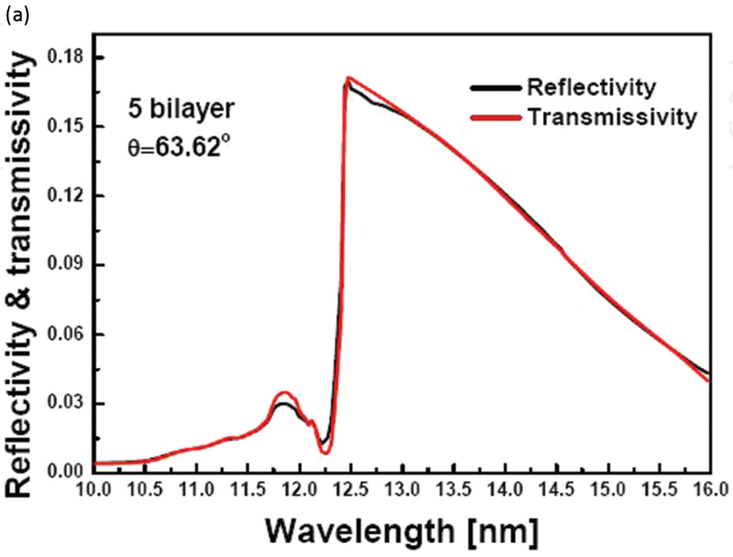

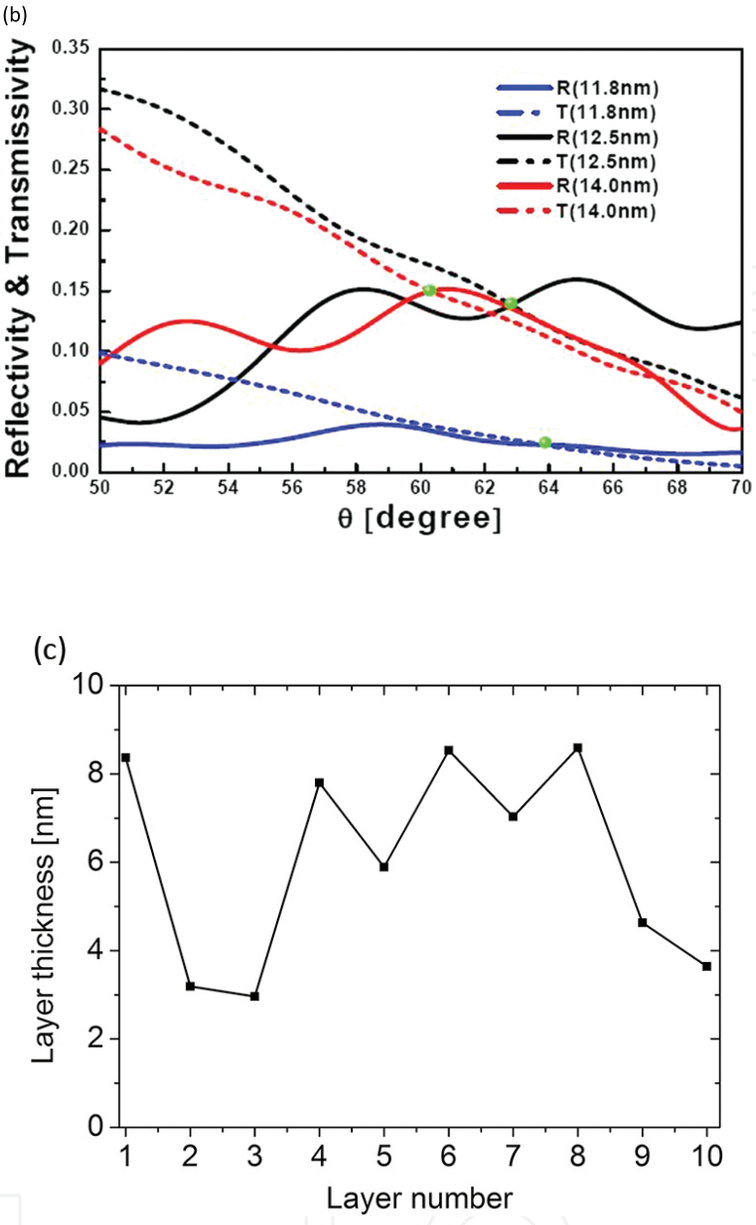

Figure 6. Reflectivity and transmitivity for a 5-bilayer Mo/Si multilayer as functions of (a) wavelength and (b) incidence angle at three different wavelengths; the green points mark the optimum angles where reflectivity and transmitivity are equal; (c) layer thickness of design.

The thicknesses of each layer and the working angle are considered as the variables of optimization. By designing with different numbers of bilayers, it was found that the intensities of reflected and transmitted beams are in best agreement for five bilayers in the wavelength range 10–16 nm, see **Figure 6(a)**. The highest intensity, which is at a wavelength slightly larger than silicon absorption edge, is about 17% and the optimal incidence angle is 63.62°. The average thicknesses of the silicon and molybdenum layers are 7.38 nm and 4.31 nm, respectively. As shown in **Figure 6(b)**, as the wavelength increases, the optimal incidence angle decreases; 63.62° is the average value. **Figure 6(c)** presents the layer thicknesses of design. Further robustness considerations [65] can be found in order to design better structures with

http://dx.doi.org/10.5772/62385

more stable optical performance when layer thickness errors are present. If a constraint condition is established before calculating the merit function, the process is stopped if the constraint becomes unsatisfied or feedback is provided to the merit function, then the optimal structure may be more robust than in normal optimization.

5. Characterization of multilayers

5.1. Introduction

Characterization of multilayers plays an important role in estimating multilayer quality and improving fabrication technology. In order to determine ultra-small layer thicknesses in multilayers, most direct and effective methods are hard X-ray grazing incidence reflection and diffuse scattering. Due to excellent penetration of hard X-rays, reflected and/or scattered X-rays produce interference fringes. If a structure is known, by using reflectivity (equation 4) or scattering (equation 5) model, the reflectivity or rocking scattering curves can be simulated. However, the inverse problems are always difficulties, especially for determining the structural parameters from diffuse scattering curves.

Reflectivity curve includes the information of layer thickness, density and interfacial width. Comparing experimental curve with theoretical curve by optimization algorithm, one can obtain these parameters. As a fitting method, in order to obtain believable results, reliable initial structure and parameter constraints are necessary. X-ray reflectivity is unable to distinguish between interfacial roughness and interdiffusion, because both deteriorate the reflectivity in a similar way. X-ray diffuse scattering is one of the most direct techniques for determining interfacial roughnesses and can also afford the information of thin film growth such as Hurst exponent and lateral/vertical correlation lengths.

In this section, curve fittings for reflectivity and diffuse scattering data are presented based on my previous studies on multilayers. These studies determined the accurate structural parameters of various material-pair multilayers and study the surface and interface performances.

5.2. Structure determination from reflectivity data

As a consumable optics, multilayer structures are not always stable. Aging effects related to the inherent characteristic of the materials deserve to be researched. Three B_4C-based multilayers [66] were deposited by using magnetron sputtering including W/B_4C, Mo/B_4C and La/B_4C multilayers. They were measured by using hard X-ray grazing incidence reflectivity while just prepared and after long-time storage in a dry atmosphere environment.

Because long-time storage may make multilayer surface oxidized and/or contaminated, in the fitting process the surface B_4C layer was regarded to have independent structural parameters from B_4C layers in interior periodic structure. Thus, there are 10 parameters need to be fitted, viz. 10 variables in the optimization, including the layer thickness, density and interface width for metal layer, B_4C layer in periodic structure and surface B_4C layer and the intensity coefficient. The fitting was based on the PSO algorithm.

As can be seen in **Table 2**, the periodic thickness increased 0.39% for La/B_4C multilayer and 0.24% for Mo/B_4C multilayer after 1 year, but decreased 0.05% for W/B_4C multilayer after 2 years. The changes may result from interdiffusion mechanism and stress release. Surface oxidation increased the stress and the changes of the layer thickness balanced the whole stress of multilayer. The outmost layer thickness increases apparently over 10% for La/B_4C and Mo/B_4C multilayers because lanthanum and molybdenum have stronger oxidation capability than tungsten so that oxygen atoms penetrate through B_4C layer gradually and react with metal atoms. The surface B_4C layer was also determined to absorb oxygen [67]. **Figure 7** shows the reflectivity and their fitting curves of La/B_4C multilayer while just prepared and after 1-year storage.

Sample	Status	Metal			B_4C			Surface B_4C		
		d [nm]	*σ* [nm]	*ρ* [% bulk]	*d* [nm]	*σ* [nm]	*ρ* [% bulk]	*d* [nm]	*σ* [nm]	*ρ* [% bulk]
W/B_4C *N* = 20	Just prepared	1.94	0.32	90.42	2.23	0.31	82.91	2.66	0.20	114.7
	2 year aged	1.93	0.32	93.70	2.23	0.31	82.62	2.61	0.21	117.8
Mo/B_4C *N* = 20	Just prepared	2.30	0.51	91.30	2.65	0.20	75.23	3.10	0.44	89.21
	1 year aged	2.30	0.49	98.70	2.66	0.18	76.90	3.33	0.58	85.87
La/B_4C *N* = 15	Just prepared	5.00	0.47	83.81	2.93	0.33	107.02	4.53	0.20	109.76
	1 year aged	5.01	0.38	82.83	2.95	0.33	105.62	5.08	0.21	90.67

Table 2. The change of the structure parameters after time aging for 3 metal/B_4C multilayers.

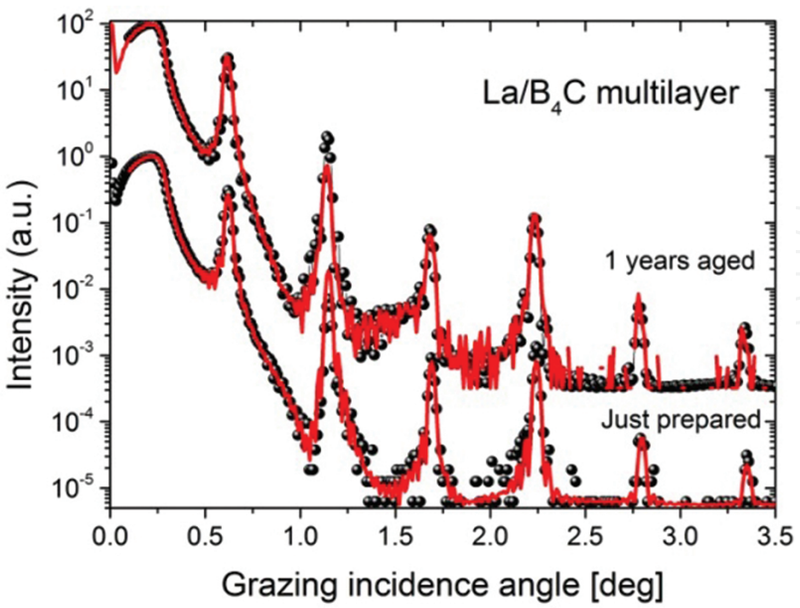

Figure 7. The grazing incidence reflectivity and their fitting curves for La/B_4C multilayer while just prepared and after 1-year storage.

http://dx.doi.org/10.5772/62385

The other previous work of structural determination is to study the stability of Ru/C multilayer monochromator with different periodic thicknesses after cryogenic cooling treatment [68]. The results show that the structural parameters keep stable after cryogenic cooling and present sufficient experimental evidences for using cryogenic-cooled multilayer monochromators in the high-thermal-load undulator beamline.

5.3. Interface investigation from diffuse scattering data

The diffuse scattering signals are distributed around the reflection direction. Common scan methods include rocking curve scans (ω scan), offset scans, detector 2θ scans and full reciprocal space scans. Rocking curve scan is by fixing the detector and scanning the incidence angle. This method is very sensitive to determine roughness information. The method of scattering curve fitting is also based on the global optimization to approach the real multilayer structure.

Sample	d [nm]	ρ [% bulk]	σ_r [nm]	σ_d [nm]	$\xi_{//}$ [nm]	h	$\xi_{\perp}$ [nm]
W/B_4C	0.83	82.10	0.29	0.10	17.19	0.10	286.64
N = 20	1.53	93.17	0.17	0.15	10.19	0.24	
Mo/B_4C	4.42	96.67	0.30	0.32	439.34	0.01	125.25
N = 30	6.06	90.07	0.14	0.17	65.86	0.07	
La/B_4C	5.01	82.81	0.35	0.32	440.56	0.01	28.32
N = 15	2.95	105.63	0.11	0.31	28.92	0.30	

Table 3. The characterization results of different metal/B_4C multilayers by using X-ray diffuse scattering technique.

Three metal/B_4C multilayers [68] were chosen to measure X-ray diffuse scattering. In order to improve the analysis precision, rocking scan curves near different Bragg maximums were fitted simultaneously. According to the fitted interfacial roughness σ_r and the interfacial width σ obtained by X-ray reflectivity measurement, the interdiffusion σ_d can be calculated by the equation $\sigma^2_d = \sigma^2 - \sigma^2_r$. As can be seen in **Table 3**, the RMS roughnesses for three multilayers are almost same, but the Mo/B_4C and La/B_4C multilayers have larger interdiffusions. Comparing the lateral correlation length $\xi_{//}$ and fractal exponent h, the Mo/B_4C and La/B_4C multilayers have stronger lateral correlation and more apparent island growth feature than the W/B_4C multilayer. Due to the weak interdiffusion and small layer thickness, the vertical correlation length in W/B_4C multilayer is over 100 times the periodic thickness. In contrast, the replication capability is very weak for La/B_4C multilayers. The vertical correlation length is only about four times the periodic thickness. **Figure 8** presents the diffuse scattering curves of Mo/B_4C multilayers and their fitting curves.

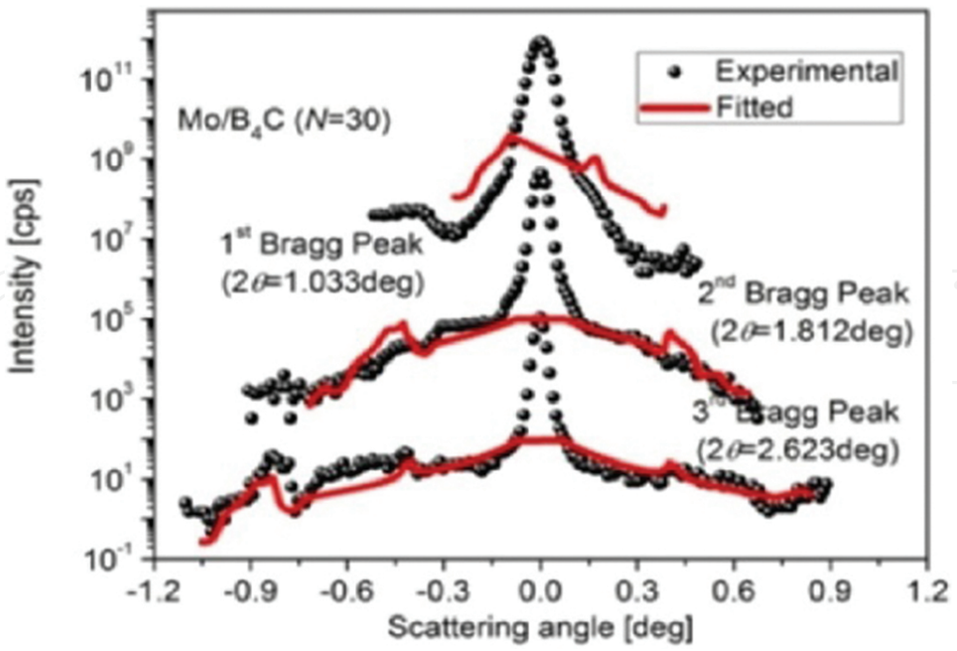

Figure 8. Rocking scan curves near three Bragg maximums and their fitted curves for Mo/B_4C multilayer ($N = 30$).

6. Conclusion

The chapter describes the effective uses of optimization algorithms in design and characterization of X-ray and EUV multilayers. Based on a suitable initial gradient structure, downhill algorithm was used to design X-ray supermirrors. The results show that supermirror can produce 15 times reflection angular range compared to periodic multilayer and increase 70% integral reflective intensity. Particle swarm optimization was used to design EUV intensity beam splitters. This kind of optics realizes equal intensities of reflected and transmitted beams in a broad spectrum around 13 nm so that exposure time decreases in EUV lithography. In the characterization of multilayers, particle swarm algorithm was successfully used to determine the slight changes of structural parameters of B_4C-based multilayers by fitting the hard X-ray grazing incidence reflectivity and diffuse scattering experimental data. This work compares the deposition technology and layer quality of different B_4C-based multilayers and helps us to know about the evolution of interfacial defects and oxidation during the aging process.

Acknowledgements

These works were supported by the National Natural Science Foundation of China (Grant No. 11304339), the Knowledge Innovation Program of Chinese Academy of Sciences and the Scientific Research Foundation for the Returned Overseas Chinese Scholars, State Education Ministry.

Author details

Hui Jiang

Address all correspondence to: jianghui@sinap.ac.cn

Shanghai Synchrotron Radiation Facility, Shanghai Institute of Applied Physics, Chinese Academy of Sciences, Shanghai, People's Republic of China

References

[1] Pelizzo MG, Suman M, Monaco G, Nicolosi P, Windt DL. Mint: High performance EUV multilayer structures insensitive to capping layer optical parameters. Optical Express. 2008;16(19):15228–15236. DOI: 10.1364/OE.16.015228

[2] Mirkarimi PB, Bajt S, Wall MA. Mint: Mo/Si and Mo/Be multilayer thin films on Zerodur substrates for extreme-ultraviolet lithography. Applied Optics. 2000;39(10):1617–1625. DOI: 10.1364/AO.39.001617

[3] Spiller E. Mint: Low-loss reflection coatings using absorbing materials. Applied Physics Letter. 1972;20(9):365–367. DOI: 10.1063/1.1654189

[4] Windt DL, Gullikson EM, Walton CC. Mint: Normal-incidence reflectance of optimized W/B_4C x-ray multilayers in the range 1.0nm<λ<2.4nm. Optics Letters. 2002;27(24): 2212-2214. DOI: 10.1364/OL.27.002212

[5] Liu WJ, Ice GE, Tischler JZ, Khounsary A, Liu C, Assoufid L, Macrander AT. Mint: Short focal length Kirkpatrick-Baez mirrors for a hard x-ray nanoprobe. Review of Scientific Instruments. 2005;76:113701. DOI: 10.1063/1.2125730

[6] Kang HC, Yan H, Winarski RP, Holt MV, Maser J, Liu C, Conley R, Vogt S, Macrander AT, Stephenson GB. Mint: Focusing of hard x-rays to 16 nanometers with a multilayer Laue lens. Applied Physics Letters. 2008;92(22):221114. DOI: 10.1063/1.2912503

[7] DuMond JWM, Youtz JP. Mint: Sensitive X-ray diffraction from artificially stratified metal films deposited by evaporation. Physical Reviews. 1935;48(8):703–703. DOI: 10.1103/PhysRev.48.703

[8] Shinjo T. Mint: Interface magnetism. Surface Science Reports. 1991;12(2):51–98. DOI: 10.1016/0167-5729(91)90010-U

[9] Vinogradov AV, Sagitov SI. Mint: New types of mirrors for the soft x-ray range (review). Soviet Journal of Quantum Electronics. 1983;13(11):1439. DOI: 10.1070/QE1983v013n11ABEH004956

[10] Barbee T, Underwood JH. Mint: Solid Fabry-Perot etalons for X-rays. Optics Communications. 1983;48(3):161–166. DOI: 10.1016/0030-4018(83)90077-9

[11] Yamamoto M, Namioka T. Mint: Layer-by-layer design method for soft-X-ray multilayers. Applied Optics. 1992;31(10):1622–1630 DOI: 10.1364/AO.31.001622

[12] Seely JF, Gutman G, Wood J, Herman GS, Kowalski MP, Rife JC, Hunter WR. Mint: Normal-incidence reflectance of W/B_4C multilayer mirrors in the 34–50-Å wavelength region. Applied Optics. 1993;32(19):3541–3547 DOI: 10.1364/AO.32.003541

[13] Yang S, Teer DG. Mint: Investigation of sputtered carbon and carbon/chromium multilayered coatings. Surface and Coatings Technology. 2000;131(1–3):412–416 DOI: 10.1016/S0257-8972(00)00859-8

[14] Kjornrattanawanich B, Bajt S, Seely JF. Mint: Multilayer-coated photodiodes with polarization sensitivity at EUV wavelength. Proceedings of SPIE. 2004;5168:31–34 DOI: 10.1117/12.507115

[15] Takenaka H, Ichimaru S, Ohchi T, Gullikson EM. Mint: Soft-X-ray reflectivity and heat resistance of SiC/Mg multilayer. Journal of Electron Spectroscopy and Related Phenomena. 2005;144–147:1047–1049. DOI: 10.1016/j.elspec.2005.01.227

[16] Kuhlmann AT, Yulin SA, Kaiser N, Bernitzki H, Lauth H. Mint: Design and fabrication of broadband EUV multilayers. Proceedings of SPIE. 2002;4688:509–515. DOI: 10.1117/12.472327

[17] Kozhevnikov I. Mint: Design of X-ray supermirrors. Nuclear Instruments and Methods in Physics Research A. 2001;460:424–443. DOI:10.1016/S0168-9002(00)01079-2

[18] Wang Z, Michette AG. Mint: Broadband multilayer mirrors for optimum use of soft x-ray source output. Journal of Optics A Pure & Applied Optics. 2000;2(5):452–457 DOI: 10.1088/1464-4258/2/5/317

[19] Wang H, Zhu J, Wang Z, Zhang Z, Zhang S, Wu W, Chen L, Michette AG, Powell AK, Pfauntsch SJ, Schafers F, Gaupp A. Mint: Broadband Mo/Si multilayer analyzers for the 15–17 nm wavelength range. Thin Solid Films. 2006;515:2523–2526. DOI: 10.1016/j.tsf.2006.04.039

[20] Wang Z, Wang H, Zhu J, Xu Y, Zhang S, Li C, Wang F, Zhang Z, Wu Y, Cheng X, Chen L, Michette AG, Pfauntsch SJ, Powell AK, Schafers F, Gaupp A, MacDonald M. Mint: Extreme ultraviolet broadband Mo/Y multilayer analyzers. Applied Physics Letters. 2006;89(24):241120. DOI: 10.1063/1.2405874

[21] Morlens A-S, Balcou P, Zeitoun P, Valentin C, Laude V, Kazamias S. Mint: Compression of attosecond harmonic pulses by extreme-ultraviolet chirped mirrors. Optics Letters. 2005;30(12):1554–1556 DOI: 10.1364/OL.30.001554

[22] Kleineberg U, Hachmann W, Heinzmann U, Hendel S, Kabachnik N, Krausz F, Neuhausler U, Uiberacker M, Uphues T, Wonisch A, Yakovlev V. Mint: Chirped

multilayer soft X-ray mirrors for attosecond soft X-ray pulses. Frontiers in Optics. San Jose, California: Springer; 2007. P409–415. DOI: 10.1007/978-1-4020-6018-2

[23] Wang H, Dhesi SS, Maccherozzi F, Cavill S, Shepherd E, Yuan F, Deshmukh R, Scott S, van der Laan G, Sawhney KJ. Mint: High-precision soft x-ray polarimeter at Diamond Light Source. Review of Scientific Instruments. 2011;82:123301. DOI: 10.1063/1.3665928

[24] Mimura H, Handa S, Kimura T, Yumoto H, Yamakawa D,Yokoyama H, Matsuyama S, Inagaki K, Yamamura K, Sano Y, Tamasaku K, Nishino Y, Yabashi M, Ishikawa T, Yamauchi K. Mint: Breaking the 10 nm barrier in hard-X-ray focusing. Nature Physics. 2010; 6(146):122–125. DOI: 10.1038/nphys1501

[25] Rack A, Weitkamp T, Riotte M, Grigoriev D, Rack T, Helfen L, Baumbach T, Dietsch R, Holz T, Kramer M, Siewert F, Meduna M, Cloetens P, Ziegler E. Mint: Comparative study of multilayers used in monochromators for synchrotron-based coherent hard X-ray imaging. Journal of Synchrotron Radiation. 2010;17: 496–510. DOI: 10.1107/S0909049510011623

[26] Eriksson F, Johansson GA, Hertz HM, Gullikson EM, Kreissig U, Birch J. Mint: 14.5% near-normal incidence reflectance of Cr/Sc x-ray multilayer mirrors for the water window. Optics Letters. 2003;28(24):2494–2496. DOI: 10.1364/OL.28.002494

[27] Jiang H, Michette AG, Pfauntsch SJ, Hart D, Shand M. Design of narrowband multilayer for Cr K_α X-rays. In: Progress In Electromagnetics Research Symposium Proceedings; 22–26 March 2010; Xi'an, China; 2010, pp. 61–65

[28] Underwood JH, Bruner ME, Haisch BM, Brown WA, Acton LW. Mint: X-ray photographs of a solar active region with a multilayer telescope at normal incidence. Science. 1987;238(4823): 61–64. DOI: 10.1126/science.238.4823.61

[29] Levashov VE, Mednikov KN, Pirzhkov AS, Ragozin EN. Mint: Aperiodic X-ray multilayer and their application in plasma spectroscopy. Radiation Physics & Chemistry. 2006;75(11):1819–1823. DOI:10.1016/j.radphyschem.2005.07.036

[30] Mishra D, Benitez M, Petracic O, Badini Confalonieri GA, Szary P, Brussing F, Theis-Brohl K, Devishvili A, Vorobiev A, Konovalov O, Paulus M, Sternemann C, Toperverg BP, Zabei H. Mint: Self-assembled iron oxide nanoparticle multilayer: x-ray and polarized neutron reflectivity. Nanotechnology. 2012;23:055707. DOI: 10.1088/0957-4484/23/5/055707

[31] Parratt LG. Mint: Surface studies of solids by total reflection of x-rays. Physical Review. 1954;95(2):359–369. DOI: 10.1103/PhysRev.95.359

[32] Croce P and Nevot L. Mint: Characterization of surfaces by grazing X-Ray reflection - application to study of polishing of some silicate-glasses. Rev Phys Appl.. 1980;503(43): 761–779. DOI: 10.1051/rphysap:01980001503076100

[33] Stepanov SA, Kondrashkina EA, Schmidbauer M, Kohler R, Pfeiffer J-U, Jach T, Souvorov AY. Mint: Diffuse scattering from interface roughness in grazing-incidence

X-ray diffraction. Physical Review B. 1996;54:8150–8162. DOI: /10.1103/PhysRevB.54.8150

[34] Sinha SK, Sirota EB, Garoff S, Stanley HB. Mint: X-ray and neutron scattering from rough surfaces. Physical Review B. 1988;38:2297–2311. DOI: 10.1103/PhysRevB.38.2297

[35] Chen L, Deng N, Zhang J. Mint: A modified quasi-Newton method for structured optimization with partial information on the Hessian. Computational Optimization and Applications. 2006;35:5–18. DOI: 10.1007/s10589-006-6440-6

[36] Petrova S and Solovev A. Mint: The origin of the method of steepest descent. Historia Mathematica 1997;24(4):361–375. DOI: 10.1006/hmat.1996.2146

[37] Levenberg K. Mint: A method for the solution of certain non-linear problems in least squares. The Quarterly of Applied Mathematics. 1944;2:164–168. DOI: 10.1515/cppm-2013-0011

[38] Marquardt DW. Mint: An algorithm for Least-Squares estimation of nonlinear parameters. Journal of the Society for Industrial and Applied Mathematics. 1963;11(2):431–441. DOI:10.1137/0111030

[39] Nelder JA, Mead R. Mint: A Simplex method for function minimization. The Computer Journal. 1965;7:308–313. DOI: 10.1093/comjnl/7.4.308

[40] Tikhonravov AV, Trubetskov MK, DeBell GW. Mint: Application of the needle optimization technique to the design of optical coatings. Applied Optics. 1996;35(28): 5493–5508. DOI: 10.1364/AO.35.005493

[41] Tikhonravov AV, Trubetskov MK, DeBell GW. Mint: Optical coating design approaches based on the needle optimization technique. Applied Optics. 2007;46(5): 704–710. DOI: 10.1364/AO.46.000704

[42] Ali MM, Storey C. Mint: Modified controlled random search algorithms. International Journal of Computer Mathematics. 1994;53:229–235. DOI: 10.1080/00207169408804329

[43] Martin S, Rivory J, Schoenauer M. Mint: Synthesis of optical multilayer systems using genetic algorithms. Applied Optics. 1995;34(13):2247–2254. DOI: 10.1364/AO.34.002247

[44] Dekkers A, Aarts E. Mint: Global optimization and simulated annealing. Mathematical Programming. 1991;50:367–393. DOI: 10.1007/BF01594945

[45] Wormington M, Panaccione C, Matney K M, Bowen D K. Mint: Characterization of structures from X-ray scattering data using genetic algorithms. Philosophical Transactions: Mathematical, Physical and Engineering Sciences. 1999;357(1761):2827–2848. DOI:10.1098/rsta.1999.0469

[46] Törn A, Viitanen S. Mint: Topographical global optimization using pre-sampled points. Journal of Global Optimization. 1994;5(3):267–276. DOI: 10.1007/BF01096456

[47] Kennedy J, Eberhart RC. Mint: Particle swarm optimization. IEEE International Conference on Neural Network. 1995;4(8):1942–1948 (1995). DOI: 10.1109/ICNN.1995.488968

[48] Dorigo M, Blum C. Mint: Ant colony optimization theory: a survey. Theoretical Computer Science. 2005;344(2–3):243–378. DOI:10.1016/j.tcs.2005.05.020

[49] Huang M, Aine CJ, Supek S, Best E, Ranken D, Flynn ER. Mint: Multi-start downhill simplex method for spatio-temporal source localization in magnetoencephalography. Electroencephalography and Clinical Neurophysiology/Evoked Potentials Section. 1998;108(1):32–44. DOI:10.1016/S0168-5597(97)00091-9

[50] Eberhart RC, Shi Y. Comparison between genetic algorithm and particle swarm optimization. In: Porto VW, Saravanan N, Waagen D, Eiben AE, editors. Evolutionary Programming VII. Berlin Heidelberg: Springer; 1998, pp. 611–616. DOI: 10.1007/BFb0040812

[51] Trelea IC. Mint: The particle swan optimization algorithm: convergence analysis and parameter selection. Information Processing Letters. 2003;85:317–325. DOI: 10.1016/S0020-0190(02)00447-7

[52] Jiang H. Characteristics of multilayer mirrors in the X-ray and extreme ultraviolet radiation ranges [thesis]. London: King's College London; 2012

[53] HΦghΦj P, Ziegler E, Susini J, Freund AK, Joensen KD, Gorenstein P, Wood JL. Mint: Focusing of hard X-rays with a W/Si supermirror. Nuclear Instruments and Methods in Physics Research B. 1997;132:528–533. DOI: 10.1016/S0168-583X(97)00437-0

[54] Boni P. Mint: Supermirror-based beam devices. Physica B: Condensed Matter. 1997;234–236:1038–1043. DOI:10.1016/S0921-4526(96)01255-0

[55] Tamura K, Yamashita K, Tawara Y, Ogasaka Y, Satake Y, Nomoto K, Okajima T. Mint: Development of supermirror telescope up to 80 keV. Proceedings of SPIE. 2003;4851:1048–1058. DOI: 10.1117/12.461318

[56] Erko A, Schafers F, Vidal B, Yakshin A, Pietsch U, Mahler W. Mint: X-ray supermirrors for BESSY II. Review of Scientific Instruments. 1995;66(10):4845–4846. DOI: 10.1063/1.1146162

[57] Wang Z, Wang H, Zhu J, Wang F, Gu Z, Chen L, Michette AG, Powell AK, Pfauntsch SJ, Schafers F. Mint: Broad angular multilayer analyzer for soft X-rays. Optics Express. 2006;14(6):2533–2538. DOI: 10.1364/OE.14.002533

[58] Wang Z, Wang H, Zhu J, Wang F, Gu Z, Chen L, Michette AG, Powell AK, Pfauntsch SJ, Schafers F. Mint: Broadband multilayer polarizers for the extreme ultraviolet. Journal of Applied Physics. 2006;99:056108. DOI: 10.1063/1.2179152

[59] Benoit N, Schroder S, Yulin S, Feigl T, Duparre A, Kaiser N, Tunnermann A. Mint: Extreme-ultraviolet-induced oxidation of Mo/Si multilayers. Applied Optics. 2008;47(19):3455–3462. DOi: doi: 10.1364/AO.47.003455

[60] Haga T, Takenaka H, Fukuda M. Mint: At-wavelength extreme ultraviolet lithography mask inspection using a Mirau interferometric microscopy. Journal of Vacuum Science & Technology B. 2000;18(6):2916–2920. DOI: 10.1116/1.1319702

[61] Budano A, Flora F, Mezi L. Mint: Analytical design method for a modified Schwarzschild optics. Applied Optics. 2006;45(18):4254–4262. DOI: 10.1364/AO.45.004254

[62] Suman M, Pelizzo MG, Nicolosi P, Windt DL. Mint: Aperiodic multilayers with enhanced reflectivity for extreme ultraviolet lithography. Applied Optics. 2008;47(16): 2906–2914. DOI: 10.1354/AO.47.002906

[63] Hiruma K, Miyagaki S, Yamanashi H, Tanaka Y, Nishiyama I. Mint: Performance and quality analysis of Mo–Si multilayers formed by ion-beam and magnetron sputtering for extreme ultraviolet lithography. Thin Solid Films. 2008;516(8):2050–2057. DOI: 10.1016/j.tsf.2007.07.182

[64] Skulina KM, Alford CS, Bionta Rm, Makowiecki DM, Gullikson EM, Soufli R, Kortright JB, Underwood JH. Mint: Molybdenum/beryllium multilayer mirrors for normal incidence in the extreme ultraviolet. Applied Optics. 1995;34(19):3727–3730. DOI: 10.1364/AO.34.003727

[65] Jiang H, Michette AG. Mint: Robust design of broadband EUV multilayer beam splitters based on particle swarm optimization. Nuclear Instruments and Methods in Physics Research A. 2013;703:22–25. DOI: 10.1016/j.nima.2012.11.038

[66] Jiang H, Wang Z, Zhu J. Mint: Interface characterization of B_4C-based multilayers by X-ray grazing-incidence reflectivity and diffuse scattering. Journal of Synchrotron Radiation. 2013;20:449–454. DOI: 10.1107/S0909049513004329

[67] Jiang H, Zhu J, Huang Q, Xu J, Wang X, Wang Z, Pfauntsch SJ, Michette AG. Mint: The influence of residual gas on boron carbide thin films prepared by magnetron sputtering. Applied Surface Science. 2011;257(23):9946–9952. DOI:10.1016/j.apsusc.2011.06.113

[68] Jiang H, He Y, He Y, Li A, Wang H, Zheng Y, Dong Z. Mint: Structural characterization and low-temperature properties of Ru/C multilayer monochromators with different periodic thicknesses. Journal of Synchrotron Radiation. 2015;22:1379–1385. DOI: 10.1107/S1600577515017828